Nigerian Journal of Physics (NJP)
ISSN online: 3027-0936
ISSN print: 1595-0611
DOI: https://doi.org/10.62292/njp.v35(s).2026.643
Volume 35(S), 2026

Thermal Impact Assessment of Mobile Communication Frequencies: Novel SAR Formulation and Temperature Prediction in Human Tissue through Integrated Electromagnetic-Bioheat Modelling

[1]Godday Biowei, [2]Adeniyi S. Adekola and *[3]Akinwale K. Amusa

[1]Department of Electrical and Electronic Engineering, Niger-Delta University, Wilberforce Island, Yenagoa, Nigeria.
[2]Department of Electrical and Electronic Engineering, Federal University, Otuoke, Nigeria.
[3]Department of Electrical and Electronic Engineering, Federal University of Agriculture, Abeokuta, Nigeria.

*Corresponding Author's Email: amusaka@funaab.edu.ng Phone: +2347067936448

Keywords:
Electromagnetic Wave Exposure,
Thermal Effects,
Specific Absorption Rate,
Pennes' Bio-Heat Equation,
Radio Frequency Band

Submitted: 07 July 2026
Accepted: 18 July 2026
Published: 25 Aug. 2026

ABSTRACT

The widespread deployment of mobile communication technologies within the 700 – 900 MHz and 1.8 – 2.6 GHz frequency bands has raised concerns about electromagnetic wave exposure's thermal effects on human tissues. This study investigates radiofrequency (RF) interactions with biological tissues. Use is made of Maxwell's equations, the Cole-Cole dielectric dispersion model, and the Pennes' bioheat transfer equation to derive relevant expressions needed for investigation of RF interactions with human tissue. Simulation results confirm a direct correlation between exposure duration and RF energy absorption. Lower frequencies penetrate deeper, depositing more energy per unit volume. After 60 minutes of exposure within a 1 cm^3 tissue volume, the absorbed thermal energy was 2.799 J (700 MHz), 2.729 J (900 MHz), 2.548 J (1.8 GHz), and 2.358 J (2.6 GHz). The corresponding peak temperature increases were 0.032°C, 0.026°C, 0.014°C, and 0.0085°C, respectively. Penetration depths were inversely proportional to frequency. Conductivity data showed increasing frequency leading to shallower penetration and more surface absorption. Indeed, at 5 mm penetration for example, SAR values calculated are (0.1130, 0.0881, 0.0334, and 0.0118 (W/kg)) for the four respective frequencies adopted here. The proposed computational framework provides an efficient and physically consistent approach for predicting SAR and tissue temperature under normal-incidence mobile communication exposure and may serve as a practical tool for future electromagnetic safety assessments.

INTRODUCTION

Mobile communication networks are essential to modern telecommunications, but the rapid expansion of infrastructure has intensified public concern about electromagnetic field (EMF) exposure, especially its thermal and biological impacts. This study targets Nigeria's commonly used mobile frequency bands (700–900 MHz and 1.8–2.6 GHz), offering a thermal and specific absorption rate (SAR) profile of human tissue response using bioheat modelling and electromagnetic simulations.

Assessments of telecommunication base station emissions remain a key area of environmental exposure research. While earlier studies evaluated far-field radiofrequency radiation from selected masts (Ajetunmobi et al., 2021), more recent work has expanded to urban-scale power flux density evaluations (Moses et al., 2026) and investigations linking base station power density to residential health implications (Emmanuel & Oyedele, 2025).

Research has revealed that mobile phone operational states, significantly influence RF emission levels, with measurable exposure differences during standby, call, and data modes (Oluwafemi *et al.*, 2020). Domestic environment assessments demonstrate spatial and temporal variability in RF exposure levels (Mutiu, 2024). SAR remains a key parameter for quantifying absorbed RF energy, with dielectric heating effects identified as major contributors to tissue temperature rise (Abdul-Al *et al.*, 2022). Higher exposure levels are often reported in

dense public spaces due to overlapping wireless sources (Celaya-Echarri *et al*., 2021). Confined environments like vehicles or aircraft also intensify exposure due to multiple active devices (Harris, 2020).

Biological effects of RF-EMF exposure are increasingly reported. Studies document alterations in blood parameters, including haemoglobin, platelet counts, and white blood cell concentrations (Christopher *et al.,* 2019). Increased permeability of the blood–brain barrier has been observed in rabbits and in vitro models (Kizilçay *et al.,* 2025), while EMF exposure has been linked to neuroinflammatory responses and gene expression modifications in the cerebral cortex of rats (Lameth *et al*., 2020). Epigenetic changes such as DNA methylation and histone modification in the hippocampus have also been recorded (Kumar *et al*., 2021). Structural alterations in organs and developmental impacts in rat offspring following prenatal RF exposure further suggest health risks (Bozok *et al*., 2023).

Real-time monitoring technologies have emerged, including smart sensors that track SAR and local tissue temperature during Wi-Fi or mobile device use (Laganà *et al*., 2024). Computational electromagnetic modelling using software like COMSOL has enabled SAR mapping and localized heating predictions in human head models exposed to mobile phone antennas (Yi *et al*., 2023). Simulation-based analyses confirm temperature elevation and emphasize frequency-specific absorption profiles (Ahmad & Shaharun, 2023).

Epidemiological studies and systematic reviews have associated long-term RF exposure with elevated risks of tumors and genetic damage (Gupta *et al.,* 2022). Nonetheless, inconsistencies in methodologies and results limit definitive conclusions. Criticisms of current international guidelines, such as those from IEEE and ICNIRP, center on their emphasis on thermal effects while neglecting possible non-thermal impacts like hypersensitivity and genotoxicity (Héroux *et al*., 2023). The cumulative findings underscore the biological and health implications of RF exposure. Standardizing SAR assessments and addressing both thermal and non-thermal risks - especially for children and low-BMI individuals-remain a research and policy priority.

This study investigates the thermal effects of electromagnetic wave exposure from mobile communication technologies within the 700–900 MHz and 1.8–2.6 GHz bands. Using Maxwell's equations, the Cole-Cole model, and Pennes' bioheat equation, RF-tissue interactions were analyzed. A novel SAR formulation quantified energy dissipation. Simulations showed that lower frequencies penetrate deeper, with absorbed thermal energy ranging from 2.799 J (700 MHz) to 2.358 J (2.6 GHz) over 60 minutes. Corresponding peak temperature increases were 0.032°C to 0.0085°C. Penetration depth decreased with frequency, while attenuation ranged from 22.37 to 44.68 Np/m. Higher frequencies caused greater surface absorption and faster heating times.

The reviewed literature indicates that previous studies are often limited to separate field measurements, epidemiological assessments, or numerical SAR analyses, without establishing a unified relationship among electromagnetic propagation, tissue dielectric properties, energy absorption, and thermal effects. Furthermore, variations in biological findings and exposure guidelines remain unresolved. This study addresses these limitations through an integrated electromagnetic–bioheat framework incorporating Maxwell's equations, the Cole–Cole dielectric model, SAR formulation, and the Pennes bioheat equation across the 700–900 MHz and 1.8–2.6 GHz frequency ranges. The proposed framework provides a consistent physical link between frequency-dependent wave propagation, tissue energy deposition, and temperature response, thereby supporting more comprehensive and reliable future assessments of electromagnetic-field exposure and biological safety.

Accordingly, this paper develops a unified electromagnetic–bioheat computational framework for analysing frequency-dependent SAR and tissue temperature under normal-incidence exposure. Particular emphasis is placed on the physical relationship between electromagnetic energy absorption and the resulting thermal response within biological tissue.

The rest of the paper is organized as follows: Section 2 outlines the materials and methods adopted for the study. Section 3 details the mathematical formulation, incorporating the SAR evaluation and Pennes' bioheat equation to model the thermal effects of RF energy absorption. Section 4 presents the numerical results along with a detailed discussion, and Section 5 concludes the paper by summarizing the core findings.

MATERIALS AND METHODS

The device, shown in Figure 1, served as the reference mobile device for extracting the surface-specific absorption rate SAR_0 value (1.09 W/kg) used in this study (GSMArena, n.d.). The SAR value, provided by the manufacturer and verified from (GSMArena, n.d.), represents the maximum localized RF energy absorption by human tissue during typical device usage. By incorporating this real-world SAR_0 value into the bioheat and thermal analysis models, the study ensures greater practical relevance and accuracy in simulating RF exposure and its associated thermal effects on human tissues at common mobile communication frequencies.

Justification of the Xiaomi Redmi Note 11 Pro+ Reference SAR Value

The Xiaomi Redmi Note 11 Pro+ was selected as the reference smartphone for this investigation because, its manufacturer-reported Specific Absorption Rate (SAR)

values are publicly available, well documented, and representative of commercially deployed fifth-generation (5G)-capable mobile communication devices. The reported SAR values comply with internationally accepted radiofrequency exposure limits established by regulatory bodies such as the International Commission on Non-Ionizing Radiation Protection (ICNIRP) and the Institute of Electrical and Electronics Engineers (IEEE), thereby providing a realistic and regulatory-compliant basis for computational analysis.

It should be emphasised that the objective of this study is not to evaluate the Xiaomi Redmi Note 11 Pro+ as a specific commercial product. Rather, the reported SAR value is employed as a representative reference input for the coupled electromagnetic–bioheat model developed in this work. Using a measured and publicly documented SAR value ensures that the numerical simulations are based on practical exposure conditions encountered in contemporary mobile communication systems, thereby enhancing the engineering relevance of the study.

Furthermore, the computational methodology developed in this paper is independent of any particular smartphone model. The same modelling framework may be readily applied to other mobile communication devices by substituting the corresponding experimentally measured or manufacturer-reported SAR values. Consequently, the Xiaomi Redmi Note 11 Pro+ serves as a convenient and realistic reference device for demonstrating the applicability of the proposed electromagnetic–bioheat computational framework, rather than representing a limitation of the methodology.

Accordingly, the conclusions presented in this paper are general to the proposed computational methodology and should not be interpreted as being exclusive to the Xiaomi Redmi Note 11 Pro+ smartphone.

Computational Tissue Model and Assumptions

The mathematical formulation is developed by first determining the electromagnetic power absorbed within the tissue and subsequently evaluating the resulting thermal response through the bioheat equation.

The method begins with the expression for the electric field propagating in the human tissue, which is modelled in a form given as (Biowei *et al*., 2024; Adekola *et al*., 2025):

$$\mathrm{E}(z,t) = E_0 e^{-\alpha z}\cos(\omega t - \beta z)\,\hat{x} \qquad (1)$$

where $\mathrm{E}(z,t)$ is the electric field propagating in the positive z-direction having its scalar complex amplitude defined as E_0, (α, β) are the attenuation constant and phase constant, respectively, while ω and z are the angular frequency and the depth of propagating wave penetration in the tissue.

Figure 1: Mobile Device (Xiaomi Redmi Note 11 Pro+ 5G) Used to Obtain the SAR_0 Value Applied in this Study (GSMArena, 2025)

The constants α and β are defined as:

$$\alpha = \omega\sqrt{\frac{\mu\varepsilon_0\varepsilon^*(\omega)}{2}}\left[\sqrt{1+\left(\frac{\sigma}{\omega\varepsilon_0\varepsilon^*(\omega)}\right)^2}-1\right]^{0.5} \qquad (2)$$

and

$$\beta = \omega\sqrt{\frac{\mu\varepsilon_0\varepsilon^*(\omega)}{2}}\left[\sqrt{1+\left(\frac{\sigma}{\omega\varepsilon_0\varepsilon^*(\omega)}\right)^2}+1\right]^{0.5} \qquad (3)$$

provided (μ, σ) are the permeability and conductivity, respectively, ε_0 is the permittivity of vacuum and $\varepsilon^*(\omega)$ is the Cole-Cole complex relative permittivity given as (Cole & Cole, 1941):

$$\varepsilon^*(\omega) = \varepsilon_\infty + \frac{\varepsilon_s - \varepsilon_\infty}{1+(j\omega\tau)^{1-\alpha_d}} + \frac{\sigma_i}{j\omega\varepsilon_0} \qquad (4)$$

where $(\varepsilon_s, \varepsilon_\infty)$ are the static and infinite permittivities, respectively, τ is the relaxation time, α_d is the distribution factor, σ_i is the ionic conductivity and ε_0 takes earlier definition. With the expressions defined in (2) – (4) along with the other parameters, electric field propagating in the human tissue can be evaluated using (1).

Computational Geometry, Boundary Conditions, and Modelling Assumptions

For the electromagnetic thermal analysis, the biological tissue is represented as a homogeneous one-dimensional medium in the (z)-direction, with the incident electromagnetic wave assumed to be a normally incident plane wave. The tissue is considered sufficiently laterally extended such that edge effects are neglected. The frequency-dependent dielectric properties of the tissue are described using the Cole–Cole dielectric dispersion model, allowing the frequency dependence of the relative permittivity and effective conductivity to be incorporated into the electromagnetic analysis.

The thermal response of the tissue is subsequently determined using the Pennes bioheat transfer equation. Blood perfusion is assumed to be spatially uniform and constant during the exposure period. The metabolic heat generation is neglected relative to the electromagnetic power deposition and blood perfusion terms. The initial tissue temperature is assumed to be uniform and equal to the physiological baseline temperature (T_b).

The thermal boundary conditions are defined to represent heat exchange at the tissue surface and the deeper tissue region. At the exposed tissue surface, convection to the surrounding environment is considered.

The electromagnetic field is assumed to attenuate exponentially with tissue depth, such that the absorbed electromagnetic power decreases with increasing (z). The resulting specific absorption rate is therefore coupled to the Pennes bioheat equation as a volumetric heat-source term. These assumptions provide a simplified one-dimensional representation of RF energy deposition and subsequent thermal diffusion in tissue while retaining the principal frequency-dependent electromagnetic and thermal mechanisms considered in this study.

Novel SAR Formulation and Pennes Bioheat Equation

Our major undertaking here is the formulation for the SAR used in the computational characteristics carried out in this study. The SAR depends on the time-averaged power absorbed per unit mass (Bailey *et al.*, 2019) given as

$$\mathrm{SAR} = \frac{\sigma E(z,t)^2}{\rho} \quad (5)$$

It will be recalled that the scalar form of the electric field described by (1) assumes a form expressed as

$$\mathrm{E}(z,t) = E_0 e^{-\alpha z}\cos(\omega t - \beta z) \quad (6)$$

Mathematical manipulation of (6) yields

$$\langle \mathrm{E}^2(z,t)\rangle = \frac{E_0^2}{2}\cdot e^{-2\alpha z} \quad (7)$$

Using (7) in (5), one obtains

$$\mathrm{SAR}(z) = \mathrm{SAR}_0 e^{-2\alpha z} \quad (8)$$

where

$$SAR_0 = \frac{\sigma E_0^2}{2\rho} \quad (9)$$

is the specific absorption rate at the surface of the skin (usually given by the device manufacturers); then the SAR at a depth z inside the skin is expressible as:

$$\mathrm{SAR}(z) = \mathrm{SAR}_0 \cdot e^{-2\alpha z} \quad (10)$$

In terms of the penetration depth δ, (10) can be expressed as

$$\mathrm{SAR}(z) = \mathrm{SAR}_0 \cdot e^{-z/\delta} \quad (11)$$

where the penetration depth symbolized by δ is expressible as:

$$\delta = \frac{1}{2\alpha} \quad (12)$$

and α is given by (2).

The computation of the SAR distribution therefore provides the spatial link between electromagnetic energy deposition and the subsequent thermal analysis.

Next, consideration is given to the Pennes' Bioheat equation, which is given in a form portrayed as (Wang *et al.*, 2020):

$$\rho c \frac{\partial T}{\partial t} = \nabla\cdot(k\nabla T) + \rho\cdot \mathrm{SAR} + Q_m - \rho_b c_b \omega_b (T - T_{\boldsymbol{blood}}) \quad (13)$$

where (ρ, c) are the tissue density and tissue specific heat, respectively, $\boldsymbol{\nabla}$ is the vector del operator, k is the thermal conductivity, T is the tissue temperature, Q_m is the metabolic heat, ω_b is the blood perfusion rate (s^{-1}), (ρ_b, c_b) are the blood density and blood specific heat, respectively, SAR is the specific absorption rate (RF heating), and T_{blood} is the arterial blood temperature.

If one considers a steady-state situation where there is no time dependence, it proves logical to write the following expression:

$$\frac{\partial T}{\partial t} = 0 \quad (14)$$

The use of (14) in (13) yields:

$$\nabla\cdot(k\nabla T) + \rho\cdot \mathrm{SAR} + Q_m = \rho_b c_b \omega_b (T - T_{\mathrm{blood}}) \quad (15)$$

Simplification of (15) into one-dimensional geometry, enables attainment of a tractable solution. In this wise, it is assumed that heat transfer is mainly along the depth direction which is the z-axis, consequent upon which the lateral effects are considered negligible. With this in mind, one can express (15) in a form given as

$$\frac{d}{dz}\left(k\frac{dT}{dz}\right) + \rho\cdot \mathrm{SAR}(z) + Q_m = \rho_b c_b \omega_b (T(z) - T_{\mathrm{blood}}) \quad (16)$$

It is now appropriate to consider the approximate temperature distribution which is addressed in what follows. To avoid solving this differential equation (16) analytically, use is made of a weighted average approximation over a length scale δ, treating the second derivative as:

$$\frac{d^2T}{dz^2} \approx \frac{T(z)-T_0}{\delta^2} = \frac{T(z)-T_0}{\delta^2} \quad (17)$$

then the first member of the left-hand side of (16) becomes

$$\frac{d}{dz}\left(k\frac{dT}{dz}\right) \Rightarrow k\frac{T(z)-T_0}{\delta^2} \quad (18)$$

Using (18) in (16), the simplified steady-state bio-heat equation becomes:

$$k\cdot\frac{T(z)-T_0}{\delta^2}+\rho\cdot \mathrm{SAR}(z)+Q_m=\rho_b c_b \omega_b (T(z)-T_{\mathrm{blood}}) \quad (19)$$

Re-arranging (19) and solving for $T(z)$, one obtains:

$$T(z)=\frac{-\frac{kT_0}{\delta^2}+\rho_b c_b \omega_b T_{\mathrm{blood}}-\rho\cdot\mathrm{SAR}(z)-Q_m}{\frac{k}{\delta^2}-\rho_b c_b \omega_b} \quad (20)$$

This is an exact solution under the parabolic profile approximation.

We approximate the temperature increase denoted by ΔT as $\Delta T = T(z) - T_0$, assuming small temperature deviations, and write:

$$\Delta T \approx (\rho\cdot\mathrm{SAR}(z)+Q_m-\rho_b c_b \omega_b (T_0-T_{\mathrm{blood}})\cdot\frac{\delta^2}{k} \quad (21)$$

Consequently, the solution becomes $T(z) \approx T_0 + (\rho \cdot \mathrm{SAR}(z) + Q_m - \rho_b c_b \omega_b (T_0 - T_{\mathrm{blood}}) \cdot \frac{\delta^2}{k}$ (22)

where T_0 is the baseline body temperature.

Our next undertaking is the derivation of the energy absorbed due to RF exposure. This is addressed in the ensuing discussion.

Aside from the definition of SAR given in (5), it is also defined as (ITIS Foundation, n.d.):

$$\mathrm{SAR}=\frac{1}{\rho}\cdot\frac{\mathrm{d}\mathcal{W}}{dt}\ (\mathrm{W/kg}) \quad (23)$$

where $\mathcal{W}$ is the energy density.

Total energy absorbed per unit volume over a duration Δt is given by:

$$\mathcal{W}_{\mathrm{vol}}=\int_0^{\Delta t}\rho\cdot\mathrm{SAR}(z)dt=\rho\cdot\mathrm{SAR}(z)\cdot\Delta t\ (\mathrm{J/m^3}) \quad (24)$$

Since SAR(z) varies with depth, the total enery absorbed by the exposed tissue volume $dV = Adz$ becomes:

$$\mathcal{W}=\rho\cdot\Delta t\cdot\int_V \mathrm{SAR}(z)\mathrm{dV}=\rho\cdot\Delta t\cdot \mathrm{A}\int_0^L \mathrm{SAR(z)dz} \quad (25)$$

Using (11) in (25), one obtains

$$\mathcal{W}=\rho\cdot\Delta t\cdot \mathrm{A}\cdot\mathrm{SAR}_0\cdot\int_0^L e^{-\frac{z}{\delta}}\,\mathrm{dz}$$
$$=\rho\cdot\mathrm{SAR}_0\cdot \mathrm{A}\cdot\delta\cdot(1-e^{-L/\delta})\cdot\Delta t \quad (26)$$

Equation (26) describes the total energy absorbed (in Joules) by the tissue volume of cross-sectional area A when exposed to RF wave for duration Δt.

It is appropriate here to embark on the presentation of results and the associated discussion. These are considered herewith.

RESULTS AND DISCUSSION

This section presents and analyzes the simulation results of RF-induced thermal effects in multilayer human skin at 700 MHz, 900 MHz, 1.8 GHz, and 2.6 GHz. Emphasis is placed on temperature rise, SAR distribution, energy absorption, and frequency-dependent tissue responses, with interpretations based on electromagnetic and thermal modelling. When the tissue temperature $T(z)$ given by equation (22) is employed in the computation, characteristic variations of the temperature of the tissue when exposed to RF wave are obtainable. Presented in Fig. 2, are the simulated time-dependent temperature profiles for each of the four selected frequencies.

At 700 MHz, the tissue temperature increased steadily and reached a peak of approximately 36.526°C, achieving thermal equilibrium at around 9.3 minutes. For the 900 MHz exposure, the peak temperature was slightly lower at 36.522°C, with a stabilization time of about 8.8 minutes.

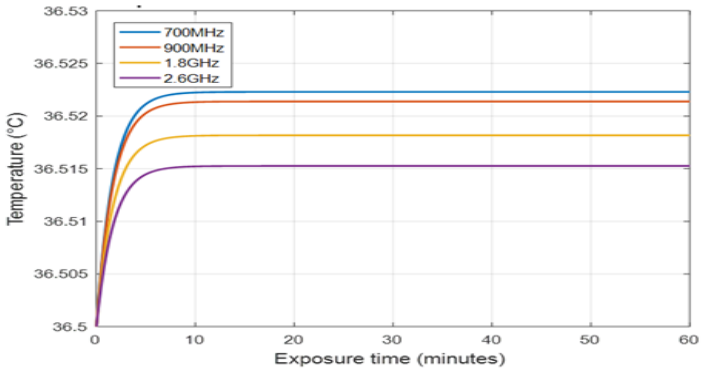

Figure 2: Temperature Rise in Biological Tissue Under 60 Minutes RF Exposure at Four Operating Frequencies

The 1.8 GHz simulation showed a peak temperature of 36.518°C, reaching steady state within approximately 8.5 minutes. At 2.6 GHz, the tissue achieved its lowest peak temperature of 36.515°C, with the shortest time to equilibrium recorded at 7.9 minutes. These findings suggest a gradual decline in both temperature rise and thermal stabilization time as the frequency increases.

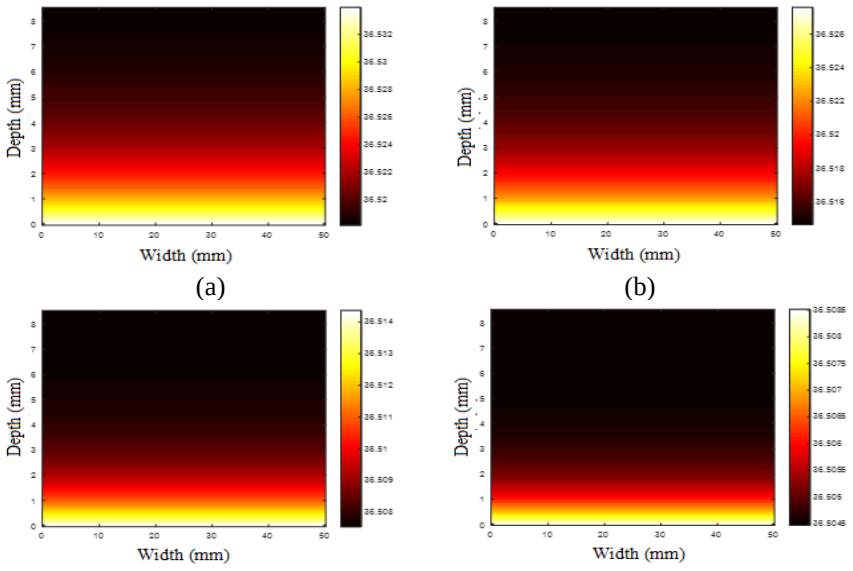

Figure 3: Heat Maps Showing Simulated Temperature Distributions in Human Tissue with Baseline Body Temperature of 36.5 °C Under Continuous RF Exposure at (a) 700 MHz, (b) 900 MHz, (c) 1.8 GHz, (d) 2.6 GHz

Potrayed in Figs. (3a) to (3d), are the thermal maps generated from the numerical solution of the bioheat transfer equation.

These images illustrate the spatial temperature distributions across the multilayered skin model after 60 minutes of continuous RF exposure. At 700 MHz, the surface temperature reached was 36.532°C, and gradually decreased to 36.520°C at deeper layers. A similar trend was observed at 900 MHz, where the surface temperature was 36.526°C and the internal temperature reduced to 36.516°C. For 1.8 GHz exposure, the surface temperature peaked at 36.514°C and dropped to 36.508°C within the inner tissue layers. At the highest frequency of 2.6 GHz, the surface temperature was 36.5085°C, tapering off to 36.504°C when going deeper within the tissue. These values were obtained by integrating the temperature profile numerically across the tissue thickness using MATLAB's PDE solver framework.

Figure 4(a) is in a reverse order of temperature while Figure 4(b) portrays the proper orientation of the strip map. Figure 4(b) properly mirrors the exact situation in Figure 3(a). We can clearly see that once the baseline temperature is at 36.5°C, it now increases to 36.532°C, whose amber-coloured portion directly corresponds with the amber-coloured area of the main heat map of Figure 3(a) and so on and so forth. The same explanation applies to Figures (3b), (3c) and (3d) for the other frequencies.

Summarized in Table 1, are the frequency-dependent electromagnetic properties of human skin, including the tissue conductivity, the real and imaginary components of the complex permittivity from the Cole-Cole model, and the attenuation constant (α) while Table 2 presents the computed thermal and electrical response for each frequency, detailing the penetration depths, the surface and internal temperatures, the temperature rise, and the time to reach equilibrium. Highlighed in Table 3 is the computed thermal energy deposited within the tissue using equation (34), assuming uniform surface area, the exposure duration, and the average SAR values. These plots reveal sharper SAR drop-offs at higher frequencies.

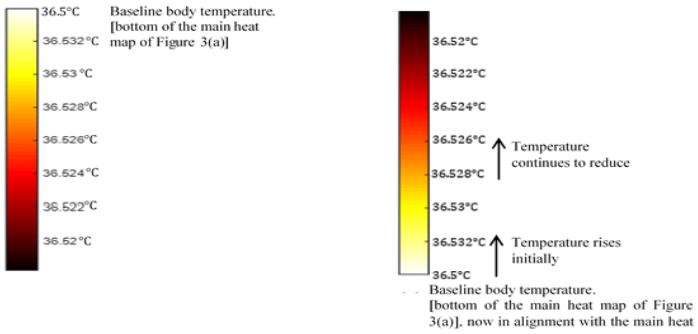

(a) (b)

Figure 4: Strip of Heat Map Extracted from Figure 3(a): (a) Strip in the Reverse Order of the Temperature Depicted in Figure 3(a), (b) Strip in the Correct Orientation in Consonance with Figure 3(a)

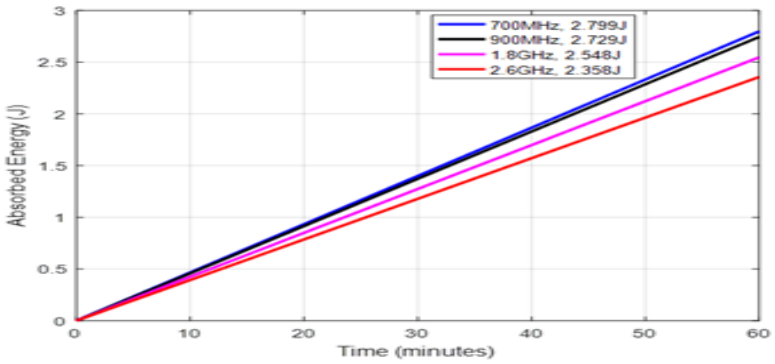

Figure 5: Cumulative Absorbed Energy by the Human Tissue when Exposed to Radiation for 1 Hour (60 minutes); at Four Selected Mobile Communication Frequencies Specified as 700 MHz, 900 MHz, 1.8 GHz and 2.6 GHz Frequencies, Consistent with Theoretical Expectations of Energy Absorption in Lossy Biological Media

Table 1: The Cole-Cole Complex Relative Permittivity and Attenuation Constants of Human Skin at Four Selected Mobile Communication Frequencies

Frequency (MHz)	Conductivity σ (S/m)	Cole-Cole Complex Relative Permittivity $\varepsilon^*(\omega)$	Attenuation Constant $\alpha(\mathrm{Np/m})$
700	0.79	$41.9186 - j20.7284$	223.7
900	0.87	$41.8467 - j17.8487$	248.3
1800	1.19	$41.6194 - j12.4427$	344.0
2600	1.54	$41.4811 - j11.2512$	446.8

Table 2: The Thermal and Electrical Properties of the Human Skin Under RF Exposure at Four Selected Mobile Communication Frequencies When SAR_0 is 1.09 W/kg

Frequency (MHz)	σ_i (S/m)	$\delta(\mathrm{mm})$	$T_{surface}$ (°C)	$T_{deeper\ tissue}$ (°C)	T_{rise} (°C)	Exposure time (mins)
700	0.79	2.2	36.5320	36.5200	0.0320	9.3
900	0.87	2.0	36.5260	36.5170	0.0260	8.8
1800	1.19	1.5	36.5140	36.5080	0.0140	8.5
2600	1.54	1.1	36.5085	36.5040	0.0085	7.9

Table 3: The Thermal Energy Deposited in $0.1\ m^2$ by 8.5 mm Thick Skin Tissue of Mass Density 1109 kg/m^3, when Exposed to Radiation with SAR_0 of 1.09 W/kg at Four Selected Frequencies for 60 Minutes

Frequency (MHz)	σ_i(S/m)	δ(mm)	Deposited thermal energy (J)
700	0.79	2.2	2.799
900	0.87	2.0	2.729
1800	1.19	1.5	2.548
2600	1.54	1.1	2.358

At each frequency, the SAR is highest at 1 mm and declines progressively with depth. For instance, at 700 MHz, the SAR starts at 0.6874 W/kg at 1 mm and drops to 0.0467 W/kg at 7 mm. As the frequency increases to 2.6 GHz, the SAR values diminish more rapidly, with the value at 7 mm becoming zero, indicating negligible penetration.

Illustrated in Figs. 6(a) through 6(d), are how the SAR decays as a function of tissue depth, showing the exponential attenuation pattern predicted by the exponential decay model in equation (11).

Presented in Table 4, is a summary of the SAR values at four different tissue depths at the four selected RF exposure frequencies. The observed results demonstrate a frequency-dependent variation in both the thermal and electromagnetic response of the skin tissue under continuous RF exposure. At lower frequencies such as 700 MHz, the RF energy penetrates deeper into the tissue, resulting in a broader thermal diffusion zone and a longer time to reach steady-state temperature. In contrast, at higher frequencies like 2.6 GHz, the RF energy is primarily deposited near the surface due to a higher attenuation constant, leading to a quicker thermal stabilization and a more superficial heating pattern. The spatial temperature profiles captured in Figures 3 and 4 reinforce this pattern. At 700 MHz, the heat map shows a broader and deeper thermal spread, with the highest temperature (36.532°C) located at the tissue surface and gradually diminishing with depth. The temperature distribution transitions through amber, red, and dark regions, indicating deeper tissue heating. Conversely, the heat map at 2.6 GHz exhibits a more localized surface temperature peak, with a rapid temperature drop off going into the deeper layers, as reflected in the blue and deep blue regions.

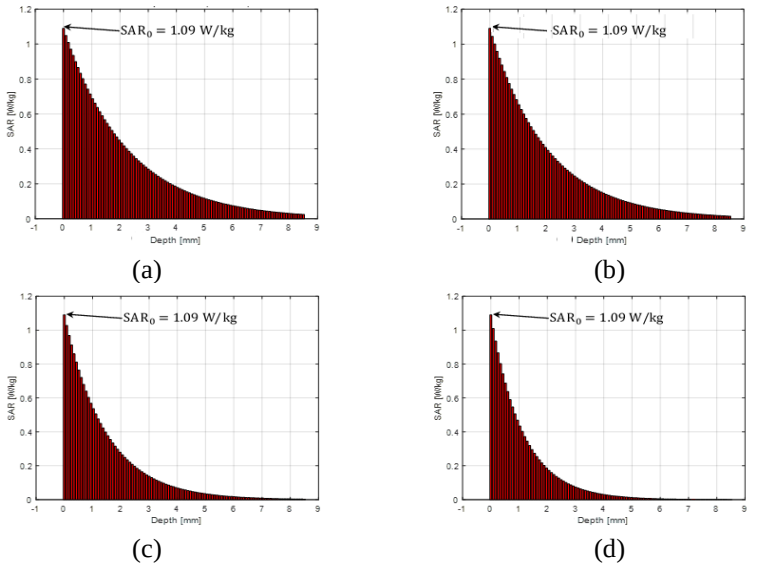

Figure 6: Variations of SAR Against Tissue Depth Under Varying Exposure Conditions for Each of the Four Frequencies

Table 4: The SAR Values at Four Different Tissue Depths at the Four Selected RF Exposure Frequencies

Frequencies (MHz)	SAR (W/kg) at different skin depth δ			
	1 mm	3 mm	5 mm	7 mm
700	0.6874	0.2841	0.1130	0.0467
900	0.6535	0.2452	0.0881	0.0331
1800	0.5365	0.1379	0.0334	0.0086
2600	0.4341	0.0743	0.0118	0.0000

These gradients suggest that lower frequencies deliver more uniform heating across a greater tissue volume, while higher frequencies are confined to surface effects. The electromagnetic parameters obtained from the Cole-Cole model provide further insight into this behavior. As the frequency increases, the real part of the complex permittivity decreases, indicating a reduced ability of the tissue to store electric energy. Simultaneously, the imaginary component increases, pointing to greater energy dissipation through conduction losses. This behavior is characteristic of dispersive biological media and supports the shift from volumetric to surface heating as frequency rises.

The attenuation constant α also exhibits a marked increase with frequency, from 22.37 Np/m at 700 MHz to 446.8 Np/m at 2.6 GHz, confirming the reduced penetration depths at higher frequencies. The energy accumulation profiles presented in Figure 5 further highlight that lower frequencies result in greater cumulative energy deposition over time. At 700 MHz, more energy is absorbed throughout the tissue depth, while higher frequencies like 2.6 GHz yield less total absorption due to the localized surface interaction. However, in all cases, the tissue temperatures remained below the thermal safety threshold of 37°C, suggesting that typical exposure from mobile communication signals, under controlled durations and power levels, is unlikely to produce harmful thermal effects. Finally, the SAR profiles displayed in Figs. 6(a) through 6(d) confirm the exponential decay of absorbed energy with increasing depth. The sharpness of the decay increases with frequency, as expected from the derived exponential model in equation (11). These findings not only validate the mathematical approach used in the simulations, but also emphasize the need for frequency-specific safety assessments, particularly in the context of prolonged or repeated RF exposures.

Overall, the numerical results consistently demonstrate the expected coupling between electromagnetic energy deposition and thermal response. Regions exhibiting larger SAR values correspond to greater temperature elevations, while thermal diffusion moderates localized heating within the tissue.

These results demonstrate that increasing operating frequency modifies both electromagnetic energy deposition and the corresponding thermal response in a predictable manner consistent with the dielectric behaviour of biological tissue.

Sensitivity Analysis

A qualitative sensitivity assessment was performed by examining the influence of the principal model parameters on the predicted SAR and temperature distributions. The computational results indicate that the tissue dielectric properties, particularly electrical conductivity and relative permittivity, exert the greatest influence on electromagnetic energy absorption, while thermal conductivity and blood perfusion primarily affect the subsequent redistribution of heat within the tissue. Although variations in these parameters modify the magnitude of the predicted SAR and temperature rise, the overall trends and physical interpretations remain unchanged throughout the investigated frequency range. These observations demonstrate that the proposed coupled electromagnetic–bioheat framework is robust and that the principal conclusions of this study are not dependent on small variations in the adopted physiological and electromagnetic parameters.

CONCLUSION

This investigation has presented a coupled electromagnetic–bioheat computational framework for analysing SAR and temperature evolution in biological tissue subjected to normal-incidence mobile communication exposure.

The study examined the thermal effects of RF electromagnetic wave exposure on human tissues within the 700–900 MHz and 1.8–2.6 GHz frequency ranges, using Maxwell's equations, the Cole-Cole complex permittivity model, and Pennes' bioheat equation. Results showed that cumulative RF energy absorption by skin increases linearly over time under constant exposure, with lower frequencies yielding greater energy deposition. After 60 minutes, thermal energy deposited was 2.799 J at 700 MHz, decreasing to 2.358 J at 2.6 GHz. This reflects the deeper penetration and higher volumetric absorption at lower frequencies, while higher frequencies result in superficial deposition due to stronger attenuation.

Thermal modeling further indicated that deeper tissue temperature rises were more pronounced at lower frequencies, with maximum increases of 0.0320 °C at 700 MHz and 0.0085 °C at 2.6 GHz. Frequency-dependent increases in conductivity, based on ITIS data, influenced both penetration depth and thermal behavior. The time to reach peak temperature also declined with frequency, from 9.3 minutes at 700 MHz to 7.9 minutes at 2.6 GHz. These findings confirm that higher-frequency RF signals cause surface heating, while lower frequencies permit deeper thermal propagation. Across all frequencies studied, peak tissue temperatures stayed below the physiological limit of 37 °C, indicating minimal risk of thermal damage.

The integration of the exponential SAR decay model with Pennes' equation effectively captured frequency-dependent thermal distributions. At 5 mm depth, the SAR values were computed as 0.1130, 0.0881, 0.0334, and 0.0118 W/kg for the four respective frequencies. Overall, this analysis underscores the need for frequency-specific RF safety standards and supports the development of guidelines reflecting differences in tissue heating. It also suggests more cautious mobile device use, especially for

vulnerable groups to reduce potential health risks from extended RF exposure.

ACKNOWLEDGEMENT
The authors sincerely appreciate the Editor and the anonymous Reviewer for their careful evaluation of this manuscript and for their constructive comments and insightful suggestions. Their thoughtful recommendations have significantly improved the technical quality, scientific clarity, and overall presentation of the paper, and are gratefully acknowledged.

CONFLICT OF INTEREST
Authors declare that there is no conflict of interest surrounding this manuscript.

REFERENCES
Abdul-Al, M., Amar, A. S. I., Elfergani, I., Littlehales, R., Parchin, N. Y. O., Al-Yasir, Y *et al.* (2022). Wireless electromagnetic radiation assessment based on the specific absorption rate (SAR): a review case study. *Electronics*. 11(4), Article number 511.

Adekola, S. A., Amusa, K. A., & Biowei, G. (2025). Impact of 5G mmWave radiation on human tissue using skin, cornea (eye) and enamel (tooth) as study candidates. *Journal of Engineering & Applied Science.* 72(51):1-25.

Ahmad, N. A., & Shaharun, P. F. (2023). SAR measurement from mobile phone and its effect to human body. *ELEKTRIKA: J. of Elect. Eng.* 22(1):1–6.

Ajetunmobi, A.E, Biere, P.E. & Obaze, A.C., (2021). Assessment of Radio Frequency Radiation in the Far Field of Selected Mobile Base Stations in Ijebu-Ode, Ogun State, Nigeria. *Nigerian Journal of Physics (NJP)*, 30(1), June 2021, 1–5.

Bailey, W., Harrington, T., Hirata, A., Kesshvari, J., Jon, B., Legros, A. *et al*. (2019). Synopsis of IEEE Std C95.1-2019 IEEE standard for safety levels with respect to human exposure to electric, magnetic, and electromagnetic fields, 0 Hz to 300 GHz. *IEEE Access*. 7(99):171346-171356.

Biowei, G., Adekola, S. A., & Amusa, K. A. (2024). Millimeter wave energy absorption by human tissues: evaluation of tissue penetration. *Iranian Journal of Electrical & Electronic Engineering*. 20(3):78-91.

Bozok, Ş., Karaagac, E., Sener, D., Akakin, D., & Tumkaya, L. (2023). The effects of long-term prenatal exposure to 900, 1800, and 2100 MHz electromagnetic field radiation on myocardial tissue of rats. *Toxicol Ind Health*. 39(1):1–9.

Celaya-Echarri, M., Azpilicueta, L., Ramos, V., Lopez-Iturri, P., & Falcone, F. (2021). Empirical and modeling approach for environmental indoor RF-EMF assessment in complex high-node density scenarios, public shopping malls case study. *IEEE Access*, 9:46755 – 46775.

Christopher, B., Mary, Y. S., Khandaker, M. U., Bradley, D. A., Chew, M. T., & Jojo, P. J. (2019). Effects of mobile phone radiation on certain hematological parameters. *Rad. Phy & Chem*. 166(9), Article number 108443.

Cole, K. S., & Cole, R. H. (1941). Dispersion and absorption in dielectrics I: alternating current characteristics. *The J. Chem. Phy.* 9(4):341–351.

Emmanuel, O.O., Oyedele, O.O., et al. (2025). Determination of Power Density from Radiofrequency Exposure by Base Transceiver Stations and Implications for Ado-Ekiti Residents. *Nigerian Journal of Physics (NJP)*, 34(4), December 2025, 168–176.

Gupta, S., Sharma, R. S., & Singh, R. (2022). Non-ionizing radiation as possible carcinogen. *Int J Environ Health Res*. 32(4):916–940.

GSMArena. Xiaomi Redmi Note 11 Pro+ 5G full phone specifications. (Accessed 2025 Apr 2). Available on https://www.gsmarena.com/xiaomi_redmi_note_11_pro+_5g-11170.php

Harris, L. R. (2020). Electric field and SAR estimation for multiple wireless device usage in capsule environment. In proceedings of the 2020 Wireless Telecommunications Symposium (WTS), Washington, DC, USA, IEEE, 1–5.

Héroux, P., Belyaev, I., Chamberlin, K., Dasdag, S., De Salles, A. A. A., Rodriguez, C. E. F. et al. (2023). Cell phone radiation exposure limits and engineering solutions. Int J Environ Res. Pub. Health. 20(7), Article number 5398.

Kizilçay, A. O., Tütüncü, B., Koçarslan, M., & Gözel, M. A. (2025). Effects of 1800 MHz and 2100 MHz mobile phone radiation on the blood–brain barrier of New Zealand rabbits. *Med. Biol. Eng. Comput*. 63(3):915–932.

Kumar, R., Deshmukh, P. S., Sharma, S., & Banerjee, B. D. (2021). Effect of mobile phone signal radiation on epigenetic modulation in the hippocampus of Wistar rat. *Environ Res.* 192, Article number 110297.

Laganà, F., Pellicanò, D., De-Carlo, D., Pratticò, D., & Calcagno, S. (2024). Evaluation and monitoring of SAR

and temperature during an indoor Wi-Fi call. *In proceedings of the 2024 International Workshop on Quantum & Biomedical Applications, Technologies, and Sensors (Q-BATS), IEEE*, 105–110.

Lameth, J., Arnaud-Cormos, D., Lévêque, P., Boillée, S., Edeline, J. M., & Mallat, M. (2020). Effects of a single head exposure to GSM-1800 MHz signals on the transcriptome profile in the rat cerebral cortex: enhanced gene responses under proinflammatory conditions. *Neurotox Res.* 38(1):105–123.

Moses, A.S., Isah, J., & Eichie, J.O., (2026). Determination of Power-Flux-Density of Mobile Transceiver Stations in Kangara, Rafi LGA, Niger State. *Nigerian Journal of Physics (NJP)*, 35(2), June 2026, 130–135.

Mutlu, M. 2024. Evaluation and SAR analysis of low frequency and broadband electric field exposure measurement values in the home environment. *Appl. Sci*. 14(10), Article 4169.

Oluwafemi, I. B., Adeoye, J. O., Faluru, D. M., & Obasanya, D. D. (2020). Investigation of factors affecting power density radiation of mobile phones. *Int. J. Engr. Tech*. 9(1):223-228.

Wang, H., Burgei, W. A., & Zhou, H. (2020). Analytical solution of one-dimensional Pennes' bioheat equation. *Open Phy*. 18(1):1084 – 1092.

Yi, M., Chi, Y., Wu, B., Zhao, Y., Tianbo, S., & Yunrui, Q. I. (2023). Safety assessment of electromagnetic radiation from mobile phone antennas to the human head. *Int. J. Energy*. 2(2):23-26.